Geophysical Research Letters

RESEARCH LETTER
10.1029/2025GL114908

First Observation of Mini Harmonic Structure in Magnetosonic Waves

Qiushuo Wang[1], Jinxing Li[1], Jacob Bortnik[1], Qianli Ma[1,2], Sheng Tian[1], Daniel N. Baker[3], John Wygant[4], George B. Hospodarsky[5], and Geoffrey D. Reeves[6]

[1]Department of Atmospheric and Oceanic Sciences, University of California, Los Angeles, CA, USA, [2]Center for Space Physics, Boston University, Boston, MA, USA, [3]Laboratory for Atmospheric and Space Physics, University of Colorado Boulder, Boulder, CO, USA, [4]School of Physics and Astronomy, University of Minnesota, Minneapolis, MN, USA, [5]Department of Physics and Astronomy, University of Iowa, Iowa City, IA, USA, [6]The New Mexico Consortium, Los Alamos, NM, USA

Key Points:

- Each harmonic of a magnetosonic wave may consist of a series of elements containing mini harmonics spaced at the O^+ gyrofrequency
- Oxygen ions are found to suppress wave generation around multiples of O^+ gyrofrequency, leading to the formation of mini harmonics
- The mini harmonic structure of wave power spectrum follows the ion Bernstein mode dispersion, confirming the wave absorption by O^+ ions

Correspondence to:
J. Li,
jinxing.li.87@gmail.com

Citation:
Wang, Q., Li, J., Bortnik, J., Ma, Q., Tian, S., Baker, D. N., et al. (2025). First observation of mini harmonic structure in magnetosonic waves. *Geophysical Research Letters*, *52*, e2025GL114908. https://doi.org/10.1029/2025GL114908

Received 16 JAN 2025
Accepted 15 MAR 2025

Abstract We recently reported the finding of elementary rising-tone emissions embedded within each harmonic of magnetosonic waves, by investigating wave electric field waveforms measured by Van Allen Probes. The present study further uncovers a new set of fine structures of magnetosonic waves, namely, each elementary rising-tone may consist of a series of mini harmonics spaced around the O^+ gyrofrequency. The measured ion distributions suggest that the proton ring distribution provides free energy to excite the waves, whilst the O^+ ions suppress the wave growth around multiples of O^+ gyrofrequency, resulting in the formation of mini harmonics. Further investigation suggests that the warm plasma dispersion relation, that is, the ion Bernstein mode instabilities, may contribute to the formation of mini harmonics. The mini harmonic structure implies a new mechanism of energy redistribution among ion species in space plasmas, potentially providing a new acceleration mechanism for O^+ ions in the magnetosphere.

Plain Language Summary Magnetosonic waves are a type of natural electromagnetic wave that helps convert and transfer energy in near-Earth space. The most striking feature of magnetosonic waves is that they consist of a series of narrow frequency bands spaced at roughly the proton gyrofrequency. Our research, using high-resolution data from NASA's Van Allen Probe satellites, discovered a fine structure within the waves. Each band consists of multiple mini bands, which we call the mini-harmonics because they are spaced around the oxygen ion (O^+) gyro-frequency at which O^+ ions naturally gyrate. The particle data measured by the satellite suggests that protons provide the free energy to generate these waves, while O^+ ions suppress the wave growth at certain frequencies, leading to the generation of mini harmonics. Our findings provide new insights on the dynamics of O^+ ions in near-Earth space.

1. Introduction

Magnetosonic waves, also known as equatorial noises (e.g., Russell et al., 1970) or ion Bernstein mode waves (e.g., Min & Liu, 2016), are electromagnetic waves found in the inner magnetosphere typically within a frequency range between the proton gyrofrequency (f_{cp}) and the lower hybrid resonance frequency (f_{LHR}) (e.g., Santolík et al., 2004). Magnetosonic waves are usually confined to the equatorial plane, and are commonly observed both inside and outside the plasmapause, distributed from the dayside to the duskside (e.g., Ma et al., 2013, 2016, 2019; Meredith et al., 2008). Magnetosonic waves can interact with radiation belt electrons through Landau resonance (Horne et al., 2007), transit-time scattering (Bortnik & Thorne, 2010), and bounce resonance (Chen et al., 2015). These processes can accelerate and scatter electrons from ~100 keV to several MeV, contributing to the formation of electron butterfly pitch angle distributions (Li & Ni et al., 2016; Maldonado et al., 2016).

A key characteristic of magnetosonic waves is their discrete harmonic structure, spaced at the proton gyrofrequency (Santolík et al., 2002). Ring current protons with a ring distribution ($\partial f / \partial v_\perp > 0$, where f represents the phase space density, and $v_\perp$ is the ion velocity perpendicular to the ambient magnetic field) at energies of around 10 keV can excite magnetosonic waves at very oblique wave normal angles (Chen et al., 2010; Ma et al., 2014). Magnetosonic waves often exhibit periodic rising-tone features, lasting for about 1 min with a frequency sweep rate of approximately 1 Hz/s (Boardsen et al., 2014; Fu et al., 2014). Observations from both Van Allen Probes (Němec et al., 2020) and Cluster satellites (Němec et al., 2015) show that these rising-tone features are compound

of multiple harmonics. A very recent study (Li et al., 2024) reveals a fine structure of magnetosonic waves, that is, each harmonic may consist of a series of "elementary" rising-tone emissions, distinct from "compound" rising-tones which extend across multiple harmonics.

Here, we further investigate the fine structure of magnetosonic waves, revealing that each harmonic consists of multiple mini-harmonics spaced around the O^+ gyrofrequency (f_{cO+}). We propose possible mechanisms to explain the mini-harmonic structure.

2. Data Description

Data provided by NASA's Van Allen Probes (Mauk et al., 2013) are investigated in this study. The Waveform Receiver (WFR) of the Electric and Magnetic Field Instruments Suite and Integrated Science (EMFISIS) (Kletzing et al., 2013) provides survey-mode wave power spectrogram. The Electric Fields and Waves (EFW) Instrument (Breneman et al., 2022; Wygant et al., 2013) provides long-term (up to ∼6 hr) burst-mode waveform with sampling rates up to 16,384 samples/s. Such long-duration waveforms offer enhanced frequency resolution compared to typical data products, enabling the resolution of wave fine structures. Ion distributions derived from the proton and oxygen fluxes measured by the Helium Oxygen Proton Electron (HOPE) (Funsten et al., 2013) and the Radiation Belt Storm Probes Ion Composition Experiment (RBSPICE) (Mitchell et al., 2013) instruments are used to analyze the wave instabilities. The geomagnetic AE and Sym-H indices from the OMNI data set are used to identify substorm and geomagnetic storm events.

3. Observations

Figure 1 presents the overview of a magnetosonic wave event. Figures 1a and 1b exhibit the AE and Sym-H indices from January 21 to 31, 2019, indicating a minor geomagnetic storm that was accompanied by several substorms. Figures 1c–1g show measurements by the WFR instrument onboard Van Allen Probe A during the recovery phase of the storm from 10:30 UT to 13:00 UT on 26 January 2019 (The vertical dashed line in Figures 1a and 1b). Figure 1c shows the ω_{pe}/ω_{ce} ratio. Figures 1d and 1e show the survey-mode wave electric spectra and the magnetic spectra, with frequency resolutions from ∼2.1 Hz at the low end to ∼100 Hz at the high end, enabling us to see the macro-structure of the waves. Magnetosonic waves were detected outside of the plasmapause, as inferred from the ω_{pe}/ω_{ce} ratio, and were observed from $L = 4.4$ to $L = 5.7$ in the afternoon sector very close to the magnetic equator. These waves exhibit rising-tone features as seen in panels d and e. The wave ellipticity in Figure 1f and the wave normal angle in Figure 1g indicate that those waves are linearly polarized and are propagating nearly perpendicularly to the ambient magnetic field, confirming that these are indeed magnetosonic waves.

The EFW burst-mode waveform is investigated to explore the detailed structure of the magnetosonic waves. Figure 2a presents the magnetic wave spectral intensity by performing the Fast Fourier Transformation (FFT) to the EFW burst-mode waveforms from 11:48 UT to 12:12 UT. The waveform cadence is 512 samples/s, and the FFT uses a window of 16,384 samples (32 s) and a shift window of 2,048 samples (4s), which provides a balance between high frequency resolution and sufficient time resolution, ensuring that mini-harmonics can be clearly identified. The resultant frequency resolution of the derived spectra is therefore 1/32 Hz, which is much higher than that of the survey-mode (∼2–100 Hz). This is the best resolution we can obtain, because the window size (32 s) is already roughly equivalent to the duration of individual emissions shown in Figure 2a.

Each harmonic of the magnetosonic wave shown in Figure 2a consists of a series of elementary rising-tone structures, similar to those reported by Li et al. (2024). A strikingly new structure evident in this figure, is that each elementary rising-tone emission consists of multiple mini harmonics. To our best estimation, these mini harmonics are spaced by around 1/16–1/13 f_{cp} where f_{cp} is the proton gyrofrequency and is seen to be about 3 Hz in this case. The spectral resolution of 1/32 Hz corresponds to about 6 data pixels per mini harmonic. Such a resolution can resolve the mini-harmonics, but may not provide an accurate gap frequency. To our best knowledge, these mini-harmonics are most likely associated with singly charged Oxygen ions (O^+) which are usually the dominant heavy ions and have a gyrofrequency f_{cO+} equal to 1/16 f_{cp}.

O^+ ions originate from the ionosphere, making a significant contribution to the plasma pressure and may even dominate over proton pressure during storm times (e.g., Daglis et al., 1999; Kistler et al., 2023; Yue et al., 2019). Previous studies reported observations of oxygen cyclotron harmonic (OCH) waves at multiples of f_{cO+} (e.g., Liu et al., 1994; Usanova et al., 2016). The OCH waves are parallel propagating, observed at frequencies starting from

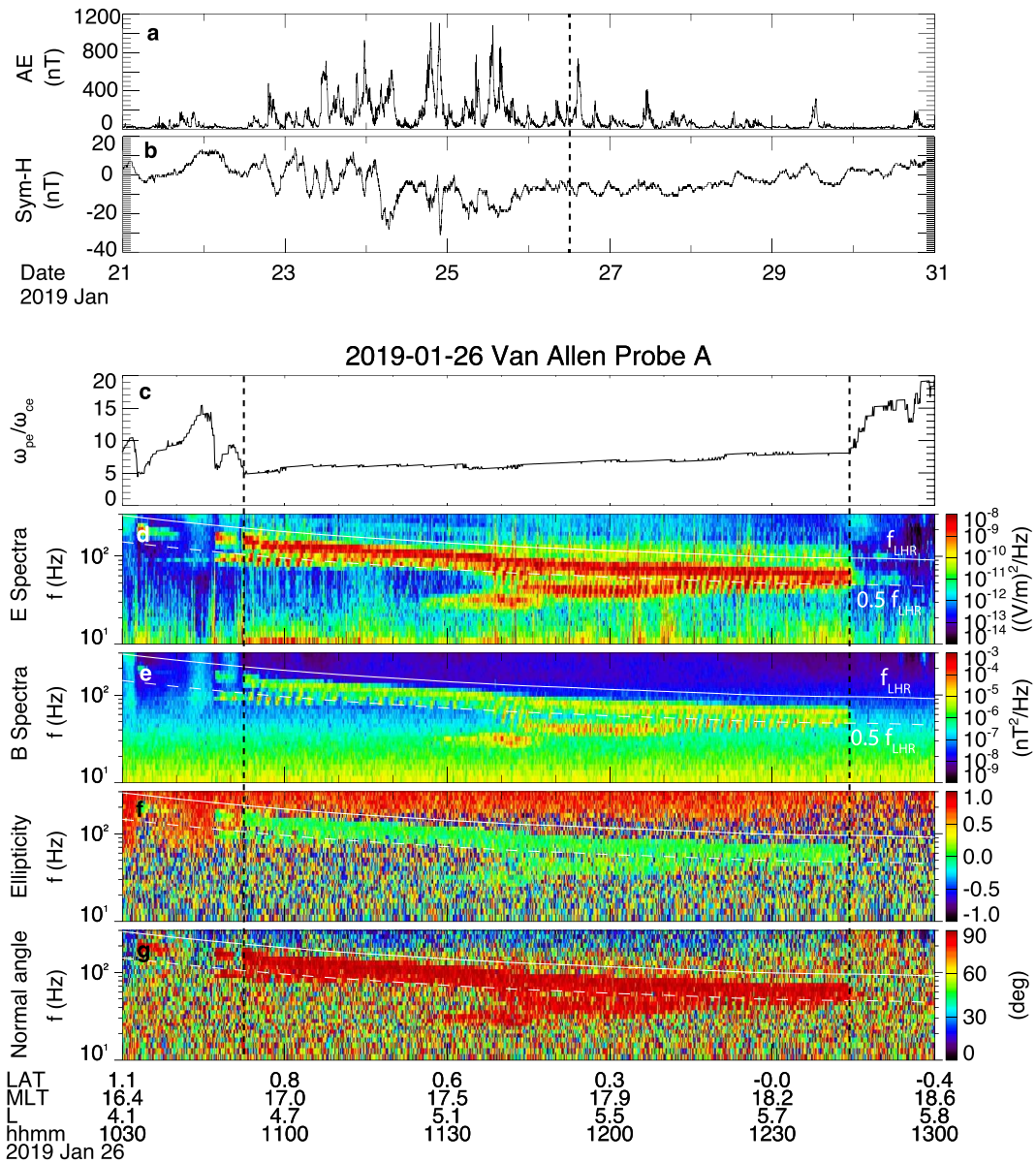

Figure 1. (a) The AE index and (b) the Sym-H index during 21–31 January 2019, with a vertical black dashed line indicating the starting moment when magnetosonic waves were observed. (c)–(g) Survey-mode measurements by the WFR instrument onboard Van Allen Probe A from 10:30 UT to 13:00 UT on 26 January 2019. Two black dashed lines in panels (c)–(g) indicate the time and location when the satellite crosses the plasmapause. (c) The ω_{pe}/ω_{ce} ratio. (d) The wave electric power spectral density and (e) the magnetic power spectral density. (f) The ellipticity and (g) the wave normal angle.

f_{cO+} to a few multiples of f_{cO+}, and with very low compressibility ($B_{\parallel}^{w} \ll B_{\perp}^{w}$, where $B_{\parallel}^{w}$ and $B_{\perp}^{w}$ are the parallel and perpendicular components of wave magnetic field) (e.g., Wang et al., 2022, 2024). These features are distinct from the magnetosonic waves with mini-harmonics that are perpendicular propagating (Figure 2b), linearly polarized (Figure 2c), observed at each f_{cp} harmonic, and highly compressible (not shown in Figure). Therefore, the mini-harmonic structure reported in this paper is a completely new phenomenon to our best knowledge.

Figure 2d displays the perpendicular proton phase space density (PSD) derived from proton differential fluxes measured by the HOPE instrument. The pink line represents the Alfven energy $E_A = m_p v_A^2/2$, where $v_A = B/\sqrt{\mu_0(m_p n_p + m_O n_O)}$, and we assumed an ion density ratio of $n_p{:}n_O$ = 0.9:0.1 (Kronberg et al., 2014; Maggiolo & Kistler, 2014). A proton ring distribution (a positive slope PSD) is seen at an energy comparable to

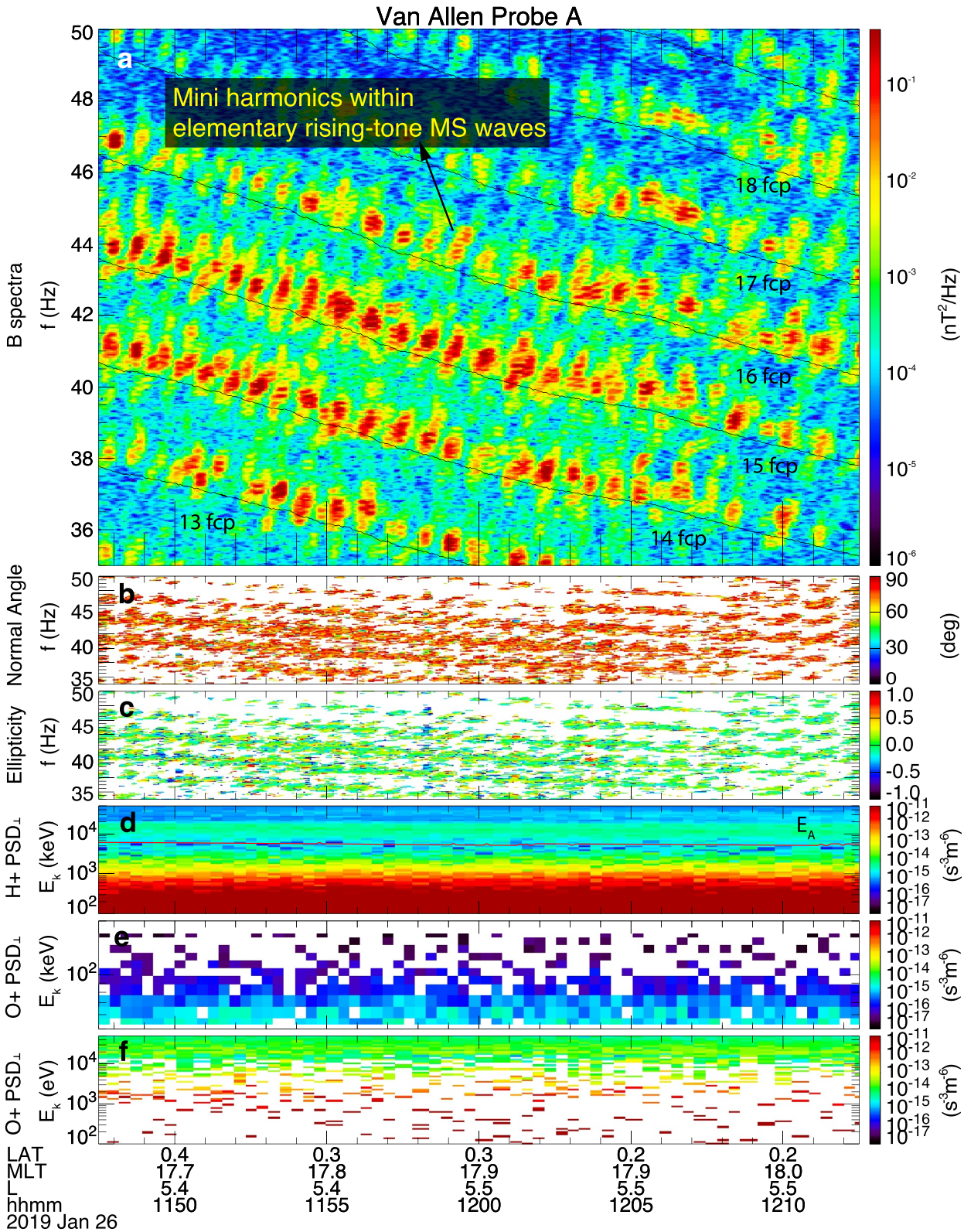

Figure 2. Burst-mode Electric Fields and Waves measurements and the corresponding ion phase space densities (PSD) from 11:47 UT to 12:13 UT on 26 January 2019. (a) Magnetic field power spectrogram, with the black solid lines indicating integer harmonics of the proton gyrofrequency (f_{cp}) ranging from 13 f_{cp} to 19 f_{cp}. (b) Wave normal angle. (c) Wave ellipticity. (d) Perpendicular proton PSD, with the red solid line indicating the Alfven energy. (e) Perpendicular O^+ PSD measured by the Helium Oxygen Proton Electron and (f) that measured by the Radiation Belt Storm Probes Ion Composition Experiment instrument.

the E_A, consistent with our understanding of the source for generating magnetosonic waves (Chen et al., 2010). Figures 2e and 2f show the perpendicular PSD of O^+ ions measured by the RBSPICE and the HOPE instruments, respectively. We do not observe a ring distribution in the O + PSD.

4. Explanation of the Mini-Harmonic Structure

To deal with the data gaps in Figure 2f which indicate no counts of O^+ ions, we average the proton and O^+ flux measurements from 11:50 UT to 12:10 UT to obtain the PSD distributions as shown in Figure 3a. The perpendicular and parallel PSDs are represented by the PSDs at 90° and 18° pitch angles, respectively. The proton PSD is based on the HOPE measurements, while O^+ PSD is obtained from a combination of the HOPE data (<52 keV), the RBSPICE-TOFxPHOHELT data product (52–139 keV, multiplied by a factor of 2 to make the PSD smooth at the overlapping energy) and the RBSPICE-TOFxEO data (142–870 keV, multiplied by a factor of 0.8).

Figure 3a clearly shows positive slopes in the proton PSDs both in the parallel and the perpendicular directions at velocities close to the Alfven velocity (~1.1 Mm/s), suggesting that the ring current protons can excite magnetosonic waves. The O^+ PSD is monotonically decreasing, indicating that they are unable to provide free energy to excite the waves. This is different from the scenario for OCH waves, where the ring distribution of hot O^+ is proposed to be the primary source (Liu et al., 2022) of free energy, and the ion Bernstein instability drives the generation of the harmonics (Liu et al., 2022; Min et al., 2017). We propose a generation mechanism for the mini harmonics that are spaced around f_{cO+}, that is, the protons with the ring distribution excite these waves, while the O^+ ions with a normal distribution suppress the waves from being generated at multiples of f_{cO+}.

We use the resonant diffusion curve (Lyons & Williams, 1984; Summers et al., 1998) to schematically illustrate the proposed mechanism. The proton ring distribution, shown in Figure 3c, tends to relax the free energy and diffuse protons toward low energies following the red arrows. To ensure efficient diffusion, the radius of the diffusion curve circle, $\omega/k_\parallel$, should be sufficiently large, and $k_\parallel$ should be sufficiently small. As a result, there is very efficient energy exchange and the ring distribution generates waves with wave normal angles very close to 90°. The oxygen ions with a normal distribution, shown in Figure 3d, absorb energy from the waves and diffuse toward higher energies where the PSD is lower, as illustrated by the red arrows. Therefore, the O^+ ions damp magnetosonic waves or suppress the waves from being generated at certain frequencies.

We utilize the linear theory of wave growth/damping to gain a basic understanding on how the O^+ ions distribution leads to the mini harmonics spaced at f_{cO+}. The averaged plasma density from 11:50 UT to 12:10 UT is 14 cm^{-3}. We assume that number density abundance of O^+ is 10% and the rest are protons. Suppose the warm component of O^+ is has a density of $n_0 = 0.2$ cm^{-3}, and follows the kappa distribution

$$f = \frac{n_0 2^{2\kappa-1}(\kappa - 1/2)\Gamma^2(\kappa)}{\pi^2\sqrt{\kappa}\Gamma(2\kappa)\, v_{T\perp}^2 v_{T\parallel}}\left(1 + \frac{v_\perp^2}{\kappa v_{T\perp}^2} + \frac{{v_\parallel}^2}{\kappa v_{T\parallel}^2}\right)^{-\kappa-1},$$

Here $(v_\perp, v_\parallel)$ are particles' perpendicular and parallel velocities, and $(v_{T\perp}, v_{T\parallel})$ the perpendicular and parallel thermal velocities. $\Gamma(\kappa)$ is the Gamma function. We adopted $\kappa = 2$, $v_{T\perp} = 80$ km/s, and $v_{T\parallel} = 60$ km/s to fit the observed O^+ ion PSD.

The linear growth rate is calculated as

$$\gamma = -\frac{D_i}{\partial D_r/\partial\omega}$$

The term D_i and D_r represent the imaginary and the real parts of the dispersion relation, respectively. For simplicity, the $\partial D_r/\partial\omega$ is approximated at the cold plasma limit, which is a commonly used approach in evaluating wave growth (e.g., Balikhin et al., 2015; Chen et al., 2010; Ma et al., 2014). Figure 3b presents the linear wave damping rates (Kennel, 1966) caused by O^+ ions as a function of frequency at wave normal angles ranging from 89.6° to 89.9°. The wave damping rates peak at nf_{cO+} while reaching their mimum at $\left(n + \frac{1}{2}\right)f_{cO+}$, especially at normal angles of 89.9°. This can be understood simply from the resonance condition equation, $\omega - k_\parallel v_\parallel = n\omega_{cO+}$ (Nunn, 1971): for magnetosonic waves with a normal angle of 89.9°, the $k_\parallel$ is small and the term $k_\parallel v_\parallel$ make little contribution, hence, the O^+ ions can only suppress magnetosonic waves at frequencies close

10.1029/2025GL114908

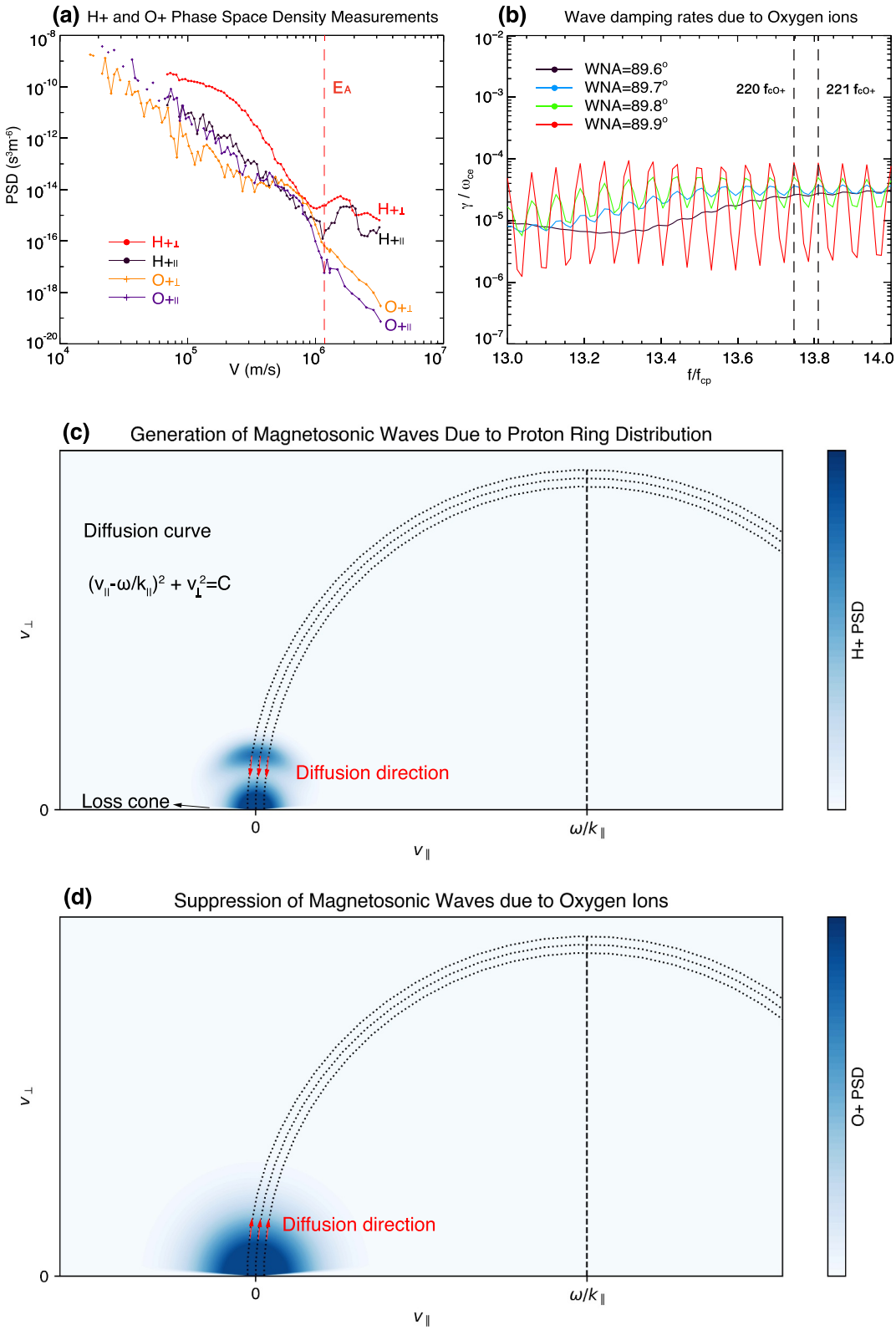

Figure 3. Illustrations and simulations of interactions between magnetosonic waves and protons and O^+ ions. (a) 20-min averaged proton and O^+ distribution measured by the Helium Oxygen Proton Electron and the Radiation Belt Storm Probes Ion Composition Experiment instruments. (b) The calculated wave damping rates caused by O^+ ions as a function of wave frequency for selected wave normal angles. (c) Schematic illustration of the excitation of magnetosonic waves due to the proton ring distribution. (d) Schematic illustration of the scenario that O^+ ions with a normal PSD distribution suppress the generation of magnetosonic waves.

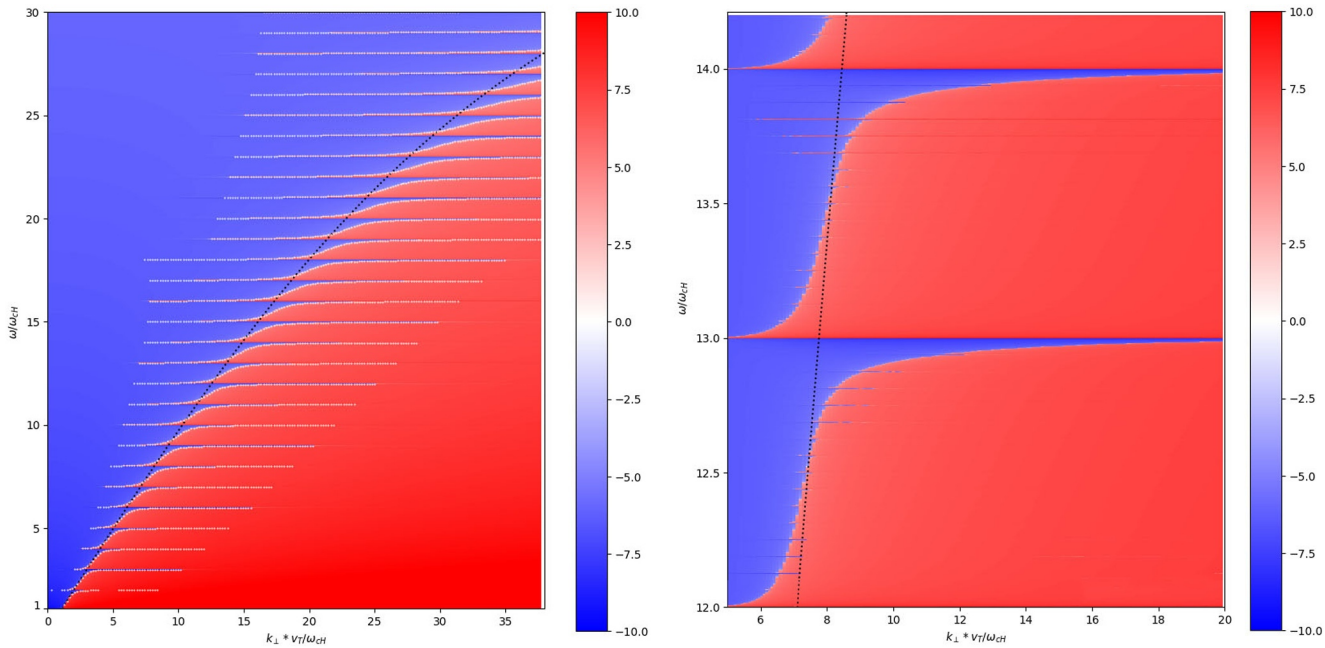

Figure 4. Dispersion relation $D(\omega, k)$ of purely perpendicular magnetosonic waves. (a) Ions are all assumed to be protons; (b) ions with an O^+ abundance of 10%. The black line represents the cold plasma dispersion relation and the white lines represent the ion Bernstein mode dispersion relation.

to nf_{cO+}. With a smaller wave normal angle, say, 89.6°, the $k_\parallel v_\parallel$ term makes a more significant contribution, and O^+ ions can effectively resonate with waves even at frequencies of $\left(n + \frac{1}{2}\right) f_{cO+}$. Such a mechanism can well explain the mini-harmonic structure for waves with a very large normal angle (~89.9°), but cannot effectively explain mini-harmonics present in waves with smaller wave normal angles. To fully explain the mini-harmonic structure, we possibly need to employ the ion Bernstein mode dispersion relation to calculate D_r and $\partial D_r / \partial \omega$.

5. Discussion

The Bernstein mode dispersion relation for protons yields branches at multiples of f_{cp}. With the inclusion of O+ ion species, we infer that the Bernstein mode may also produce secondary branches at multiples of f_{cO+}. Figure 4a illustrates the purely perpendicularly propagating ion Bernstein mode dispersion waves $D(\omega, k)$ without O^+ and Figure 4b shows this dispersion relation with O^+. In the proton-only case, we assume the protons consist of a cold population and a warm population. The red areas in the figure indicate positive values of D and the blue negative values. The waves can only exist at $D(\omega, k) = 0$, indicated by the white lines in Figure 4a. The harmonics in the solution may play a critical role in forming the harmonic structure at multiples of f_{cp}. The black dashed line represents the cold plasma dispersion relation, which agrees with the Bernstein mode well at low frequencies, but differs significantly at high frequencies.

In the two ion species scenario, we assume an O^+ number density abundance of 10%, and the O+ ions consist of a cold component (20%) and a warm component (80%). The calculated Bernstein mode solution, shown in Figure 4b, exhibits ordinary harmonics at multiples of f_{cp}, and within each ordinary harmonic, we see gaps at multiples of f_{cO+}. We note that Figure 4b shows the dispersion relation for purely perpendicular propagating waves ($k_\parallel = 0$) which are relatively easy to calculate, and the gaps at multiples of f_{cO+} are very small. A comprehensive calculation at other wave normal angles is needed to fully understand the Bernstein mode waves and the generation of mini-harmonics, and it will be left for future work due to its complexity. But a purely perpendicular solution serves as a good approximation of magnetosonic waves which tend to cluster around very oblique (~90°) wave normal angles.

6. Conclusions

This study presents newly discovered mini-harmonic structures embedded within magnetosonic waves found in Earth's magnetosphere, by investigating the EFW burst-mode waveform measured by Van Allen Probes. We show that mini-harmonics are observed within elementary rising-tone emissions in each harmonic of a magnetosonic wave. We summarize our findings and the simulation results as follows:

1. Each harmonic of a magnetosonic wave consists of many mini-harmonics spaced around the O^+ gyrofrequency. Such a mini-harmonic structure is observed in magnetosonic waves both with and without elementary rising-tone emissions.
2. The observed proton and O^+ phase space densities in association with mini-harmonics suggest that protons with a ring distribution provide the free energy to excite magnetosonic waves, while O^+ ions with a normal distribution suppress the waves from being amplified at multiples of the O^+ gyrofrequency, thereby creating the mini-harmonic structure.
3. We suggest that the ion Bernstein mode instability needs to be considered to understand the generation of the mini-harmonic structure.

The discovery of the fine structure of magnetosonic waves provides new insights into the energy transfer between different ion species, and potentially introduces a new acceleration mechanism of O^+ ions in the inner magnetosphere. While the contribution of heavy ions has usually been neglected in modeling magnetosonic waves, this study shows the direct signature of their existence, and highlights the importance of including O^+ ions in the model. Our preliminary survey indicates that mini-harmonics are commonly observed in the magnetosonic waves (not shown in this paper), possibly because O^+ ions are significantly enhanced and become the dominant heavy ion species during storm times. Due to the prevalence of the mini-harmonic structure, a comprehensive statistical analysis with all available data is suggested, which will undoubtedly lead to a far deeper understanding of magnetosonic waves and O^+ ion dynamics.

Data Availability Statement

The EFW waveform (https://rbsp.space.umn.edu/rbsp_efw/) and EMFISIS wave data (Kletzing, 2022) are publicly available. The proton and oxygen ion distributions measured by the HOPE instrument are publicly available from Funsten (2022). The geomagnetic indices are available through the OMNI database (https://spdf.gsfc.nasa.gov/pub/data/omni/high_res_omni/).

Acknowledgments
JL and JB acknowledge NASA Grants LWS-80NSSC20K0201, 80NSSC21K0522, 80NSSC18K1227, NNX14AI18G, and the Grant DE-SC0010578. QM acknowledges the NASA Grant 80NSSC24K0572 and NSF Grant AGS-2225445. This work is supported by RBSP-ECT and EMFISIS funding provided by JHU/APL contract No. 967399 and 921647 under NASA's prime contract No. NAS5-01072.

References

Balikhin, M. A., Shprits, Y. Y., Walker, S. N., Chen, L., Cornilleau-Wehrlin, N., Dandouras, I., et al. (2015). Observations of discrete harmonics emerging from equatorial noise. *Nature Communications*, *6*(1), 7703. https://doi.org/10.1038/ncomms8703

Boardsen, S. A., Hospodarsky, G. B., Kletzing, C. A., Pfaff, R. F., Kurth, W. S., Wygant, J. R., & MacDonald, E. A. (2014). Van Allen Probe observations of periodic rising frequencies of the fast magnetosonic mode. *Geophysical Research Letters*, *41*(23), 8161–8168. https://doi.org/10.1002/2014GL062020

Bortnik, J., & Thorne, R. M. (2010). Transit time scattering of energetic electrons due to equatorially confined magnetosonic waves. *Journal of Geophysical Research*, *115*(A7), A07213. https://doi.org/10.1029/2010JA015283

Breneman, A. W., Wygant, J. R., Tian, S., Cattell, C. A., Thaller, S. A., Goetz, K., et al. (2022). The Van Allen Probes electric field and waves instrument: Science results, measurements, and access to data. *Space Science Reviews*, *218*(8), 69. https://doi.org/10.1007/s11214-022-00934-y

Chen, L., Maldonado, A., Bortnik, J., Thorne, R. M., Li, J., Dai, L., & Zhan, X. (2015). Nonlinear bounce resonances between magnetosonic waves and equatorially mirroring electrons. *Journal of Geophysical Research: Space Physics*, *120*(8), 6514–6527. https://doi.org/10.1002/2015JA021174

Chen, L., Sun, J., Lu, Q., Gao, X., Xia, Z., & Zhima, Z. (2016). Generation of magnetosonic waves over a continuous spectrum. *Journal of Geophysical Research: Space Physics*, *121*(2), 1137–1147. https://doi.org/10.1002/2015JA022089

Chen, L., Thorne, R. M., Jordanova, V. K., & Horne, R. B. (2010). Global simulation of magnetosonic wave instability in the storm time magnetosphere. *Journal of Geophysical Research*, *115*(A11), A11222. https://doi.org/10.1029/2010JA015707

Daglis, I. A., Thorne, R. M., Baumjohann, W., & Orsini, S. (1999). The terrestrial ring current: Origin, formation, and decay. *Reviews of Geophysics*, *37*(4), 407–438. https://doi.org/10.1029/1999rg900009

Fu, H. S., Cao, J. B., Zhima, Z., Khotyaintsev, Y. V., Angelopoulos, V., Santolík, O., et al. (2014). First observation of rising-tone magnetosonic waves. *Geophysical Research Letters*, *41*(21), 7419–7426. https://doi.org/10.1002/2014GL061867

Funsten, H. O. (2022). Van allen Probe A energetic particle, composition, and thermal plasma suite (ECT) Helium oxygen proton electron, HOPE, mass spectrometer pitch angle resolved science data. Electron fluxes, 15 eV to 50 keV, and ion fluxes, 1 eV to 50 keV, as measured in alternate spin cadence, level 3, release #4 (L3), 11.35 s data [Dataset]. *NASA Space Physics Data Facility*. https://doi.org/10.48322/17p9-rf75

Funsten, H. O., Skoug, R. M., Guthrie, A. A., MacDonald, E. A., Baldonado, J. R., Harper, R. W., et al. (2013). Helium, oxygen, proton, and electron (HOPE) mass spectrometer for the Radiation Belt Storm Probes mission. *Space Science Reviews*, *179*(1–4), 423–484. https://doi.org/10.1007/s11214-013-9968-7

Horne, R. B., Thorne, R. M., Glauert, S. A., Meredith, N. P., Pokhotelov, D., & Santolik, O. (2007). Electron acceleration in the Van Allen radiation belts by fast magnetosonic waves. *Geophysical Research Letters*, *34*(17), L17107. https://doi.org/10.1029/2007GL030267

Kennel, C. (1966). Low-frequency whistler mode. *Physics of Fluids*, *9*(11), 2190–2202. https://doi.org/10.1063/1.1761588

Kistler, L. M., Asamura, K., Kasahara, S., Miyoshi, Y., Mouikis, C. G., Keika, K., et al. (2023). The variable source of the plasma sheet during a geomagnetic storm. *Nature Communications*, *14*(1), 6143. https://doi.org/10.1038/s41467-023-41735-3

Kletzing, C. A. (2022). Van Allen Probe A WFR waveform data [Dataset]. *NASA Space Physics Data Facility*. https://doi.org/10.48322/13VC-C837

Kletzing, C. A., Kurth, W. S., Acuna, M., MacDowall, R. J., Torbert, R. B., Averkamp, T., et al. (2013). The electric and magnetic field instrument suite and integrated science (EMFISIS) on RBSP. *Space Science Reviews*, *179*(1–4), 127–181. https://doi.org/10.1007/s11214-013-9993-6

Kronberg, E. A., Ashour-Abdalla, M., Dandouras, I., Delcourt, D. C., Grigorenko, E. E., Kistler, L. M., et al. (2014). Circulation of heavy ions and their dynamical effects in the magnetosphere: Recent observations and models. *Space Science Reviews*, *184*(1–4), 173–235. https://doi.org/10.1007/s11214-014-0104-0

Li, J., Bortnik, J., Thorne, R. M., Li, W., Ma, Q., Baker, D. N., et al. (2016). Ultrarelativistic electron butterfly distributions created by parallel acceleration due to magnetosonic waves. *Journal of Geophysical Research: Space Physics*, *121*(4), 3212–3222. https://doi.org/10.1002/2016JA022370

Li, J., Bortnik, J., Tian, S., Ma, Q., An, X., Ma, D., et al. (2024). Fine structure of magnetospheric magnetosonic waves: 1. Elementary rising-tone emissions within individual harmonic. *Journal of Geophysical Research: Space Physics*, *129*(3), e2024JA032462. https://doi.org/10.1029/2024JA032462

Li, J., Ni, B., Ma, Q., Xie, L., Pu, Z., Fu, S., et al. (2016). Formation of energetic electron butterfly distributions by magnetosonic waves via Landau resonance. *Geophysical Research Letters*, *43*(7), 3009–3016. https://doi.org/10.1002/2016GL067853

Liu, H., Kokubun, S., & Hayashi, K. (1994). Equatorial electromagnetic emission with discrete spectra near harmonics of oxygen gyrofrequency during magnetic storm. *Geophysical Research Letters*, *21*(3), 225–228. https://doi.org/10.1029/93GL02836

Liu, X., Chen, L., Sun, J., Wang, X., & Usanova, M. E. (2022). A parametric study of oxygen ion cyclotron harmonic wave excitation and polarization by an oxygen ring distribution. *Journal of Geophysical Research: Space Physics*, *127*(11), e2022JA030828. https://doi.org/10.1029/2022JA030828

Lyons, L. R., & Williams, D. J. (1984). *Quantitative aspects of magnetospheric physics*. D. Reidel Co. https://doi.org/10.1007/978-94-017-2819-5

Ma, Q., Li, W., Bortnik, J., Kletzing, C. A., Kurth, W. S., Hospodarsky, G. B., & Wygant, J. R. (2019). Global survey and empirical model of fast magnetosonic waves over their full frequency range in earth's inner magnetosphere. *Journal of Geophysical Research: Space Physics*, *124*(12), 270–282. https://doi.org/10.1029/2019JA027407

Ma, Q., Li, W., Chen, L., Thorne, R. M., & Angelopoulos, V. (2014). Magnetosonic wave excitation by ion ring distributions in the Earth's inner magnetosphere. *Journal of Geophysical Research: Space Physics*, *119*(2), 844–852. https://doi.org/10.1002/2013JA019591

Ma, Q., Li, W., Thorne, R. M., & Angelopoulos, V. (2013). Global distribution of equatorial magnetosonic waves observed by THEMIS. *Geophysical Research Letters*, *40*(10), 1895–1901. https://doi.org/10.1002/grl.50434

Ma, Q., Li, W., Thorne, R. M., Bortnik, J., Kletzing, C. A., Kurth, W. S., & Hospodarsky, G. B. (2016). Electron scattering by magnetosonic waves in the inner magnetosphere. *Journal of Geophysical Research: Space Physics*, *121*(1), 274–285. https://doi.org/10.1002/2015JA021992

Maggiolo, R., & Kistler, L. M. (2014). Spatial variation in the plasma sheet composition: Dependence on geomagnetic and solar activity. *Journal of Geophysical Research: Space Physics*, *119*(4), 2836–2857. https://doi.org/10.1002/2013JA019517

Maldonado, A. A., Chen, L., Claudepierre, S. G., Bortnik, J., Thorne, R. M., & Spence, H. (2016). Electron butterfly distribution modulation by magnetosonic waves. *Geophysical Research Letters*, *43*(7), 3051–3059. https://doi.org/10.1002/2016GL068161

Mauk, B. H., Fox, N. J., Kanekal, S. G., Kessel, R. L., Sibeck, D. G., & Ukhorskiy, A. (2013). Science objectives and rationale for the radiation BeltStorm Probes mission. *Space Science Reviews*, *179*(1–4), 3–27. https://doi.org/10.1007/s11214-012-9908-y

Meredith, N. P., Horne, R. B., & Anderson, R. R. (2008). Survey of magnetosonic waves and proton ring distributions in the Earth's inner magnetosphere. *Journal of Geophysical Research*, *113*(A6). https://doi.org/10.1029/2007JA012975

Min, K., Denton, R. E., Liu, K., Gary, S. P., & Spence, H. E. (2017). Ion Bernstein instability as a possible source for oxygen ion cyclotron harmonic waves. *Journal of Geophysical Research: Space Physics*, *122*(5), 5449–5465. https://doi.org/10.1002/2017JA023979

Min, K., & Liu, K. (2016). Understanding the growth rate patterns of ion Bernstein instabilities driven by ring-like proton velocity distributions. *Journal of Geophysical Research: Space Physics*, *121*(4), 3036–3049. https://doi.org/10.1002/2016JA022524

Mitchell, D. G., Lanzerotti, L. J., Kim, C. K., Stokes, M., Ho, G., Cooper, S., et al. (2013). Radiation Belt Storm Probes Ion Composition Experiment (RBSPICE). *Space Science Reviews*, *179*(1–4), 263–308. https://doi.org/10.1007/s11214-013-9965-x

Němec, F., Santolík, O., Hrbáčková, Z., Pickett, J. S., & Cornilleau-Wehrlin, N. (2015). Equatorial noise emissions with quasiperiodic modulation of wave intensity. *Journal of Geophysical Research: Space Physics*, *120*(4), 2649–2661. https://doi.org/10.1002/2014JA020816

Němec, F., Tomori, A., Santolík, O., Boardsen, S. A., Hospodarsky, G. B., Kurth, W. S., et al. (2020). Fine harmonic structure of equatorial noise with a quasiperiodic modulation. *Journal of Geophysical Research: Space Physics*, *125*(3), e2019JA027509. https://doi.org/10.1029/2019JA027509

Nunn, D. (1971). Wave-particle interactions in electrostatic waves in an inhomogeneous medium. *Journal of Plasma Physics*, *6*(2), 291–307. https://doi.org/10.1017/S0022377800006061

Russell, C. T., Holzer, R. E., & Smith, E. J. (1970). OGO 3 observations of ELF noise in the magnetosphere: 2. The nature of the equatorial noise. *Journal of Geophysical Research*, *75*(4), 755–768. https://doi.org/10.1029/JA075i004p00755

Santolík, O., Němec, F., Gereová, K., Macúšová, E., de Conchy, Y., & Cornilleau-Wehrlin, N. (2004). Systematic analysis of equatorial noise below the lower hybrid frequency. *Annals of Geophysics*, *22*(7), 2587–2595. https://doi.org/10.5194/angeo-22-2587-2004

Santolík, O., Pickett, J. S., Gurnett, D. A., Maksimovic, M., & Cornilleau-Wehrlin, N. (2002). Spatiotemporal variability and propagation of equatorial noise observed by Cluster. *Journal of Geophysical Research*, *107*(A12), 1495. https://doi.org/10.1029/2001JA009159

Summers, D., Thorne, R. M., & Xiao, F. (1998). Relativistic theory of wave-particle resonant diffusion with application to electron acceleration in the magnetosphere. *Journal of Geophysical Research*, *103*(A9), 20487–20500. https://doi.org/10.1029/98JA01740

Usanova, M. E., Malaspina, D. M., Jaynes, A. N., Bruder, R. J., Mann, I. R., Wygant, J. R., & Ergun, R. E. (2016). Van Allen Probes observations of oxygen cyclotron harmonic waves in the inner magnetosphere. *Geophysical Research Letters*, *43*(17), 8827–8834. https://doi.org/10.1002/2016GL070233

Wang, Y., Liu, K., Cheng, K., Mousavi, A., Yao, F., Wang, X., & Wang, R. (2024). Generation mechanism of oxygen ion cyclotron harmonic waves in the inner magnetosphere: Linear instability analysis based on observations. *Geophysical Research Letters*, *51*(24), e2024GL112168. https://doi.org/10.1029/2024GL112168

Wang, Y., Liu, K., Min, K., Yao, F., Xiong, Y., Cheng, K., et al. (2022). Van Allen Probes observations of oxygen ion cyclotron harmonic waves: Statistical study. *Geophysical Research Letters*, *49*(4), e2021GL096825. https://doi.org/10.1029/2021GL096825

Wygant, J. R., Bonnell, J. W., Goetz, K., Ergun, R. E., Mozer, F. S., Bale, S. D., et al. (2013). The electric field and waves instrument on the Radiation Belt Storm Probes mission. *Space Science Reviews*, *179*(1–4), 183–220. https://doi.org/10.1007/s11214-013-0013-7

Yue, C., Bortnik, J., Li, W., Ma, Q., Wang, C.-P., Thorne, R. M., et al. (2019). Oxygen ion dynamics in the Earth's ring current: Van Allen Probes observations. *Journal of Geophysical Research: Space Physics*, *124*(10), 7786–7798. https://doi.org/10.1029/2019ja026801